

PROJECT REPORT:  
PRELIMINARY FEASIBILITY STUDY OF PETRACK

By Marc Chamberland  
#100727230

Work submitted to  
Dr. Tong Xu  
for the course  
PHYS 4909

Department of Physics  
Faculty of Science  
Carleton University  
Friday, April 20<sup>th</sup>, 2007

**Table of Contents**

Introduction..... 3

PeTrack Overview..... 3

System Setup..... 4

Estimation of Detector Resolution ..... 5

Data Extraction ..... 6

Results ..... 8

Discussion..... 11

Conclusion ..... 13

References..... 15

## **Introduction**

The purpose of this study was to perform a preliminary assessment of the accuracy and feasibility of PeTrack, a positron emission marker based real-time tumor tracking technique. We proceeded by using a clinical Positron Emission Tomography (PET) system and a modified version of the tumor tracking algorithm to locate the position of a single Ge-68 line source. Although some key piece of information is still missing, the computed locations and standard deviations seem to support this proof of concept experiment.

## **PeTrack Overview**

Radiotherapy is commonly used for palliative or therapeutic treatment of cancer patients. Because of the damaging nature of the radiation used, it is important to minimize normal tissue exposure. However, abdominal tumor motion due to breathing limits the delivery accuracy of radiotherapy. Thus, techniques that enable high precision locating of moving tumors due to respiratory motion are required.

The PeTrack technique aims to accurately track the 3-D position of the tumor inside the patient using positron emission markers. The markers are cylindrical capsules of 0.5-0.8 mm in diameter and 2-4 mm in length and contain a point-like low activity positron emission source. Their small size makes them easy to implant in tumors. The detection of annihilation gamma rays allows calculating the position of the markers. Indeed, when the two photons interact with detector elements, then the annihilation must have occurred close to the straight line joining both detectors. This line is called the coincidence line or line of response (LOR).

For the case of a single marker, positron emission particle tracking (PEPT) can be used to accurately track its position by detecting two pairs of back-to-back gamma rays. The point at which these two reference lines cross correspond approximately to the location of the source. As in PET, positron range, photon noncollinearity and scatter events may degrade the accuracy of the method. Positron range refers to the distance from the emitting source that the positron travels before annihilating. Photon noncollinearity is the emission of annihilation gamma rays at an angle less than  $180^\circ$  due to residual kinetic energy and momentum from the positron-electron pair at annihilation. Accuracy can be improved by collecting a larger number of coincidence lines.

The location of the point source is determined as the point in space that minimizes the root mean square distance to the coincidence lines.

To track tumor movement however, multiple fiducial markers are needed. Consequently, the numerous coincidence lines need to be assigned to the correct marker. PeTrack's tumor tracking method uses an iterative Expectation-Maximization clustering algorithm for this purpose. The distance between a coincidence line and its emission source is assumed to follow a Gaussian distribution with a certain standard deviation and mean zero. An initial estimate of the markers' locations is made and using the Gaussian distribution, the probability of each coincidence line belonging to a particular cluster is computed. If the coincidence line is too far away (more than two standard deviations), it is discarded. Subsequently, the parameters are updated and the assumed position of the source is adjusted using a vector weighted with the probabilities. The iterations stop once the change in location of the source is less than 0.05 mm.

For more details about these methods, see references.

## System Setup

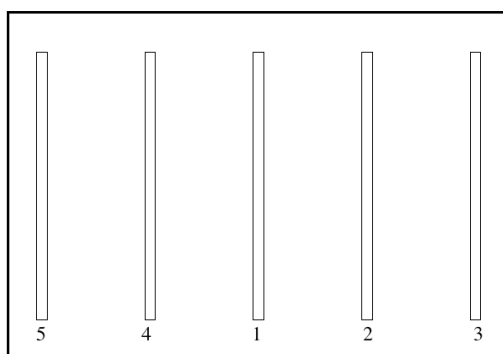


Figure 1 Schematic of acrylic plate. Distance between indentations is approximately 1.6 cm.

Although in practice PeTrack would use specially designed gamma ray detectors, for the purpose of this experiment, a simple PET system was used to acquire data. Thus the experiment was conducted at the University of Ottawa Heart Institute using a clinical PET ECAT ART system and a Ge-68 line source, with active core diameter of 1.52 mm and overall diameter 3.02 mm. The activity of the source was measured to be 1 mCi on April 1<sup>st</sup>, 2006. The source rested

on an acrylic plate into one of five evenly spaced numbered indentations (see Figure 1). The plate was placed approximately in the middle of the detector ring - although its exact position was not recorded - so that the line source was parallel to the axis of the PET scanner. In this configuration, the source can be regarded approximately as a point source because data is recorded in 3.375 mm wide slices.

PET systems usually require a full ring detector in order to record data from every possible angle. However, the PET system used in this experiment consisted of two opposed partial ring detectors. These detectors revolve about the scanner axis to cover a full 180 degrees. While in PET this rotation is required to record radioactive activity distribution in a patient, during this experiment, the rotation of the detectors was turned off in order to simulate the PeTrack geometry. The data acquisition time was set to 1 s, the minimum value that seemed achievable on this system. A PET scanner actually consists of a series of adjacent detector rings. Coincidences detected within the same detector ring create a direct coincidence plane. However, sensitivity can be improved by adding the coincidence events from adjacent detector rings to create cross-planes of coincidence. In our case, the maximum ring difference was set to 1, so that cross-planes recorded twice as many events as the direct planes, as shown on Figure 2.

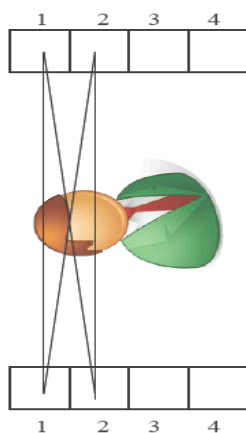


Figure 2 Direct planes and cross-planes between rings 1 and 2

## Estimation of Detector Resolution

The intrinsic spatial resolution of the detector system used is limited mainly by three factors: positron range, photon noncollinearity and detector crystal width. The finite size of the line

source also limits the achievable resolution. The following estimates the intrinsic resolution of the system:

$$\sigma_d = \sqrt{(\sigma_c^2 + \sigma_p^2 + \sigma_r^2 + \sigma_s^2)}$$

$\sigma_c = d/2$  relates to the crystal where  $d$  is the crystal width ( $d = 0.675$  cm);  $\sigma_p = 0.0022D$  relates to photon noncollinearity where  $D$  is the detector ring diameter ( $D = 82$  cm);  $\sigma_r$  relates to the positron range ( $\sigma_r \sim 1$  mm);  $\sigma_s = R$  relates to the line source where  $R$  is the active core radius ( $R = 0.76$  mm). This yields an intrinsic detector resolution of  $\sigma_d = 8.57$  mm.

## Data Extraction

Raw data from the experiment had to be converted to a format usable by the tumor tracking program. The individual pixel values from the matrix scan file format obtained from the PET system were converted to 4-byte floats using `ecat2flo 1.0.1` by Turku PET Center (see references). The open-source image processing software ImageJ was then used to view and manipulate the data of the five images, containing 47 slices each. The distance between slices is 0.3375 cm. Figure 3 (left) shows slice 28 when the line source was placed in the middle position. In this 192 x 192 image, called a sinogram, each pixel represents one LOR, with the pixel value corresponding to the number of events recorded (the count). The vertical axis corresponds to the angle between the LOR and the x-axis, while the horizontal axis corresponds to the shortest distance between the center of the detector ring of radius  $R$  and the LOR. Figure 3 (right) shows the area delimiting possible LOR. Possible coincidence lines can be determined by the geometry of Figure 4, where  $D$  is the two opposite detector arcs and 1 and 2 represent two different LOR. LOR 2' illustrates that at the maximum angle, only one LOR is possible.

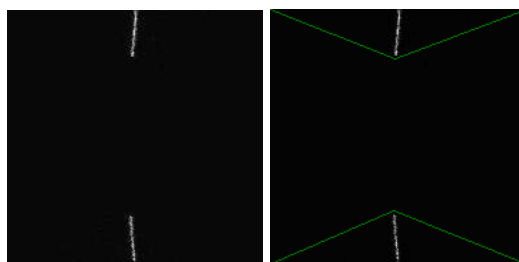


Figure 3 Position #1, slice 28 (left); area delimiting possible LOR (right)

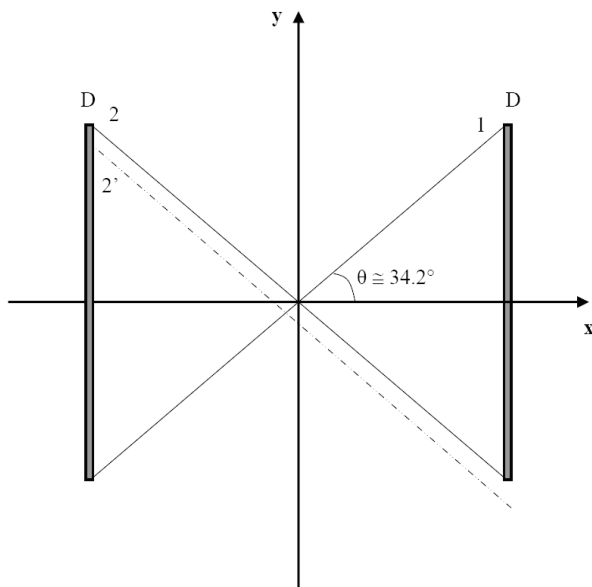


Figure 4 Possible LOR

Figure 5 shows the geometry of the PET system in question. The z-axis comes out of the page. For a fixed value of theta, the distance between two consecutive lines of response is 0.3375 cm (X res. on Figure 5). Similarly, the angle value increases by  $(180^\circ/192) = 0.9375^\circ$ . Using this geometry, an ImageJ plug-in was written to calculate and output the count value and the start and end points of each coincidence line. The tumor tracking algorithm then used the output to calculate the position of the source. However, certain changes were made to the tumor tracking algorithm. In particular, the probability of a certain coincidence line corresponding to a cluster was weighted by its count value.

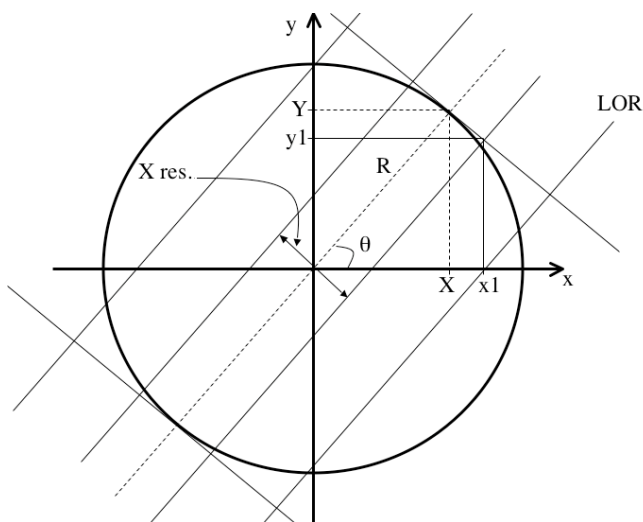


Figure 5 Geometry of detector system

## Results

The position of the source was calculated for each slice from 20 to 30 for each of the five positions. The line source was not visible outside this range of slices. The position of the plate inside the PET system was not recorded, so it is not possible to compare the computed locations of the line source with its real position.

Figure 6 and Figure 7 show the calculated locations for positions 3 and 4 on the acrylic plate in function of slice number. From the geometry of the source, it follows that the positions calculated should follow a linear fit. The standard error on these positions was calculated as the standard deviation from the fitted curve. Standard deviations on x for the five positions on the plate range from 0.33 to 0.95 mm with an average of 0.63 mm. Standard deviations on y range from 0.14 to 0.26 mm with an average of 0.19 mm. Linear regression data ( $Y = A + B \cdot X$ ) can be found in Table 1, where SD is the standard deviation.

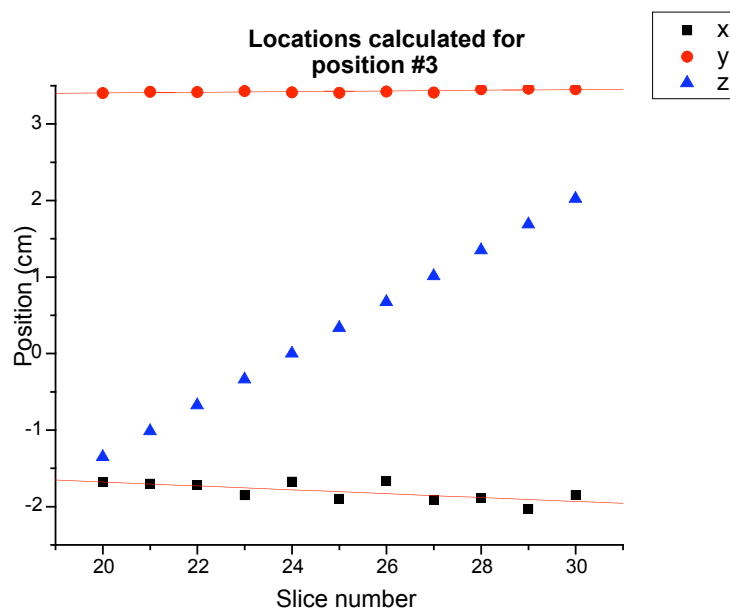


Figure 6 Calculated positions for position #3

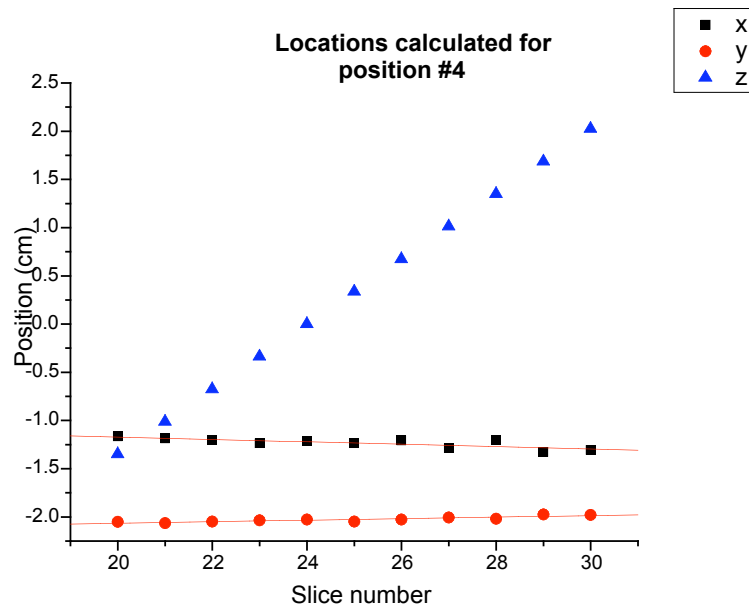


Figure 7 Calculated locations for position #4

Table 1 Linear regression data for positions 3 and 4

Position 3	Parameter	Value	Error	Position 4	Parameter	Value	Error
x	A	-1,17363	0,23003	x	A	-0,92359	0,08003
	B	-0,02531	0,00913		B	-0,01244	0,00318
	SD	0,09574			SD	0,03331	
	N	11			N	11	
y	A	3,31611	0,03568	y	A	-2,22335	0,03299
	B	0,00441	0,00142		B	0,00787	0,00131
	SD	0,01485			SD	0,01373	
	N	11			N	11	

Figure 8 and Figure 9 show position calculated for slice 26 and 29, respectively, with error bars corresponding to the previously calculated standard deviations. Each point corresponds to a different position of the source on the plate. Linear fit data is included on each graph.

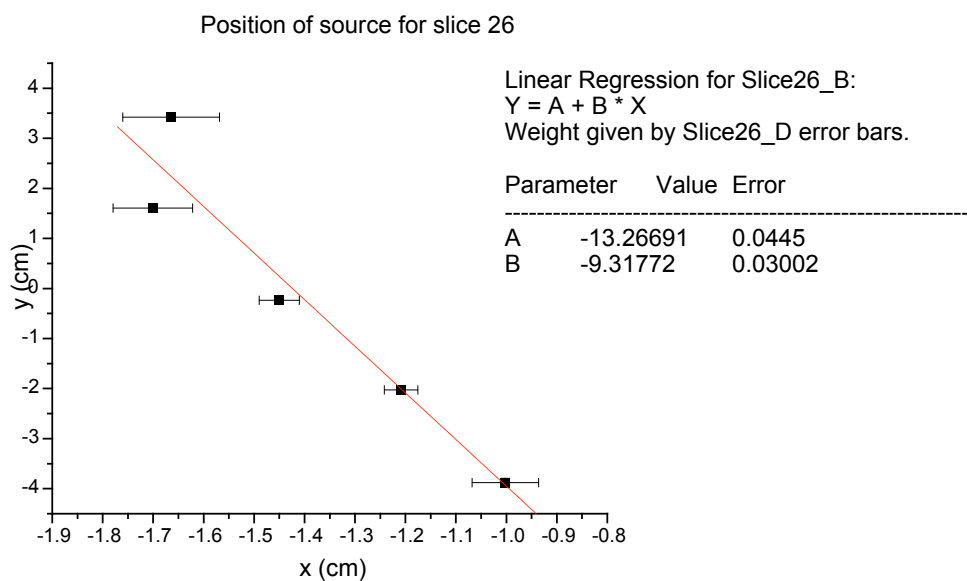


Figure 8 Source position, slice 26

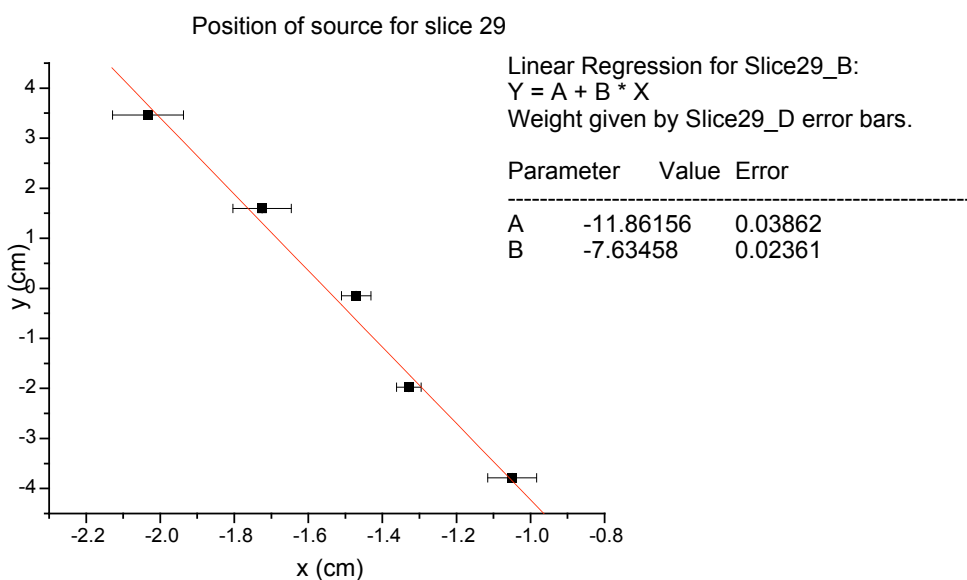


Figure 9 Source position, slice 29

Although the experiment was conducted with only one line source at a time, it is possible to simulate the tracking of two or more markers simultaneously. This was accomplished by merging the dataset of three different positions on the acrylic plate (positions 1, 2 and 4) and using this new dataset with the PeTrack algorithm. Furthermore, the order of the lines of data in the merged

file was randomized using a shuffler that permutes the lines in a text file. This was done to further simulate acquisition data of three markers. For each slice, the algorithm ran using a specified number of counts ranging from 100 to 4100. Successive iterations of the algorithm were made until the total number of counts (~6000) was reached. The average scatter fraction over all runs was 0.24. Once again, the standard deviation on the x and y coordinates of the markers were taken to be the standard deviation from the linear fit of the position as a function of slice number. The average standard deviation as a function of counts per marker used is shown in Figure 10. It can be seen that the standard deviation quickly falls below the 1 mm range when approximately 200 counts per marker are used by the algorithm.

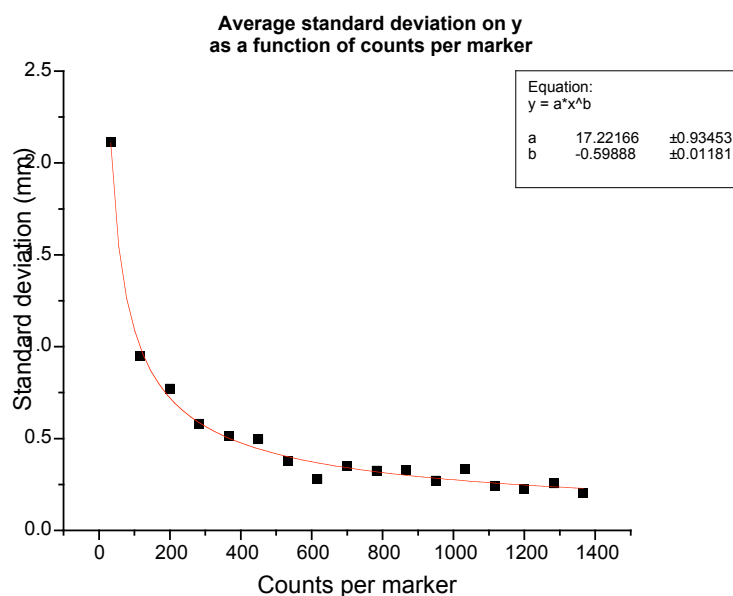


Figure 10 Average standard deviation on y as a function of counts per marker

## Discussion

As predicted by the simulation study (Xu et al., 2006), standard deviations were found to be in the sub-millimeter range. The error on x was found to be greater than the error on y. This was expected by choosing the x-axis to be perpendicular to the detector face. Indeed, the finite crystal width introduces an uncertainty on the normal direction, as seen on Figure 11.

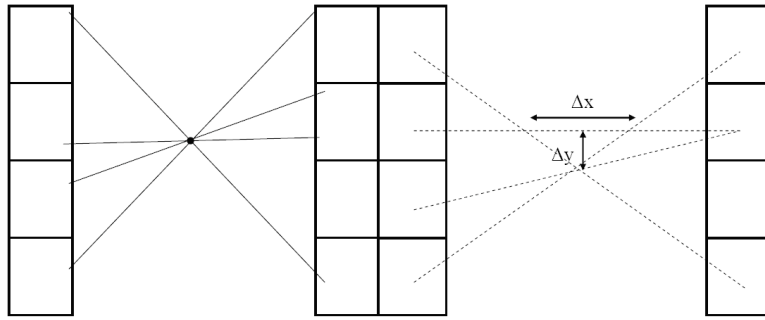


Figure 11 Left: photons can hit any part of the detector elements; right: the system records these events as LOR joining the centers of the detector elements

Moreover, there exists a geometrical relation between the error on  $x$  and  $y$ . Figure 12 shows that a blurring along  $y$  will cause a similar blurring along  $x$ , and vice versa. Because we're dealing with average errors and ideally the number of events would not vary significantly along the detector face, we can take the angle of this geometry to be half the half-width of the detector face, that is  $\theta \cong 34.2^\circ / 2 = 17.1^\circ$ . Using our average  $y$ -error, we find an  $x$ -error of  $\Delta x \cong \Delta y / \tan \theta = (0.19 \text{ mm}) / \tan (17.1^\circ) = 0.62 \text{ mm}$ . This is very close to our calculated average standard deviation on  $x$  of 0.63 mm.

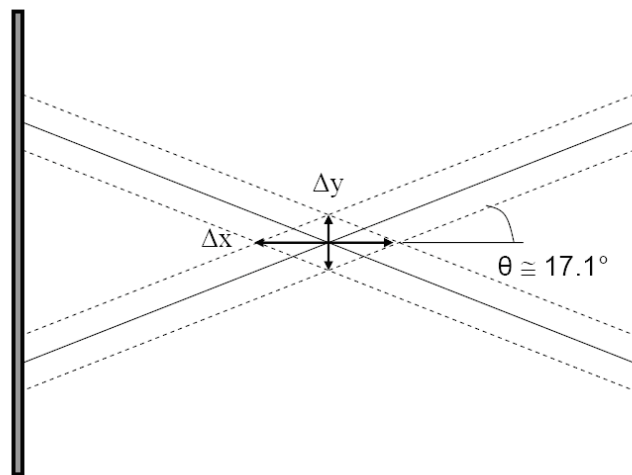


Figure 12 Geometrical relation between error on  $x$  and  $y$

The use of a line source instead of a point one contributed to the error as well. This particular uncertainty can be estimated and compared to the standard deviations obtained. Using for example the linear fit of position 4, the uncertainty on  $x$  for a certain slice is given by  $0.1244 \times 3.375 \text{ mm} = 0.42 \text{ mm}$ , which is very much comparable to the standard deviation of 0.33 mm

achieved for this particular choice of position and slice. Similarly, in  $y$  we obtain an uncertainty of  $0.0787 \times 3.375 \text{ mm} = 0.266 \text{ mm}$ , again in the same range as the one from the linear fit ( $\sim 0.14 \text{ mm}$ ). This effect could be added to the intrinsic detector resolution, however it is negligible compared to the other contributions.

Figure 10 showed the decrease in standard deviation with respect to the number of counts per marker used by the algorithm. This agrees with the assumption that higher counts will yield a better localization accuracy. In fact, for this particular kind of algorithm, it can be shown (Parker et al., 1993) that the accuracy ideally follows  $\sigma_d / \sqrt{N}$ , where  $N$  is the number of coincidence lines. Figure 13 indeed shows that our calculated standard errors follow loosely the same kind of law. Only for very low counts do our distribution differ greatly from the theoretical values. This could possibly be attributed to the inherent difficulty of localizing markers with so few counts. Parker et al. (1993) also suggest that a small sampling size does not present ideal statistical behavior. In this case, it would be expected that the data deviate from the ideal distribution.

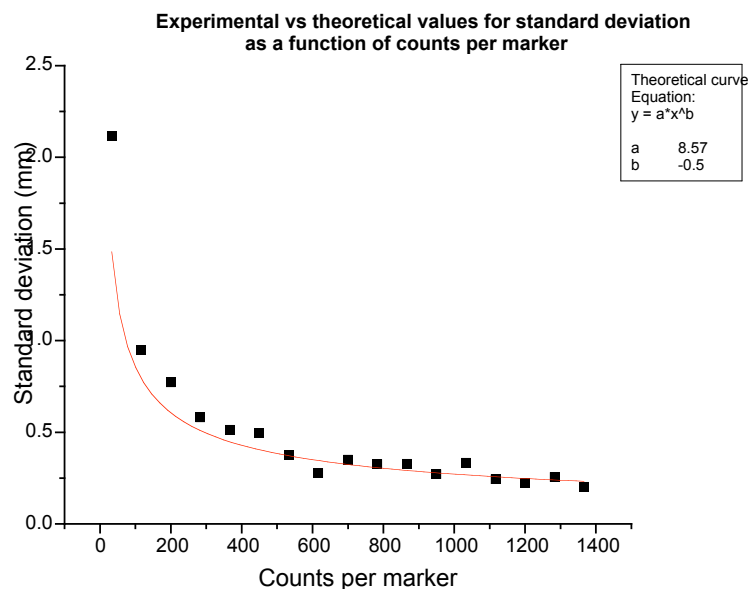


Figure 13 Experimental standard deviations versus theoretical curve

## Conclusion

Using a clinical PET system and a single line source, it has been shown that PeTrack can indeed achieve submillimeter accuracy in localizing up to three markers simultaneously.

Although the exact positions were not recorded, the error analysis seem to agree with the previous simulation study performed, giving an average standard variation on x of 0.63 mm and on y, of 0.19 mm. Furthermore, the standard deviation decreases with the number of counts per marker used by the algorithm, as expected.

The next step in the study will be to test the algorithm using three point sources moving at different speeds on an inclined spinning disk. Although the experiment has already been conducted, results are still pending analysis.

## References

- DL Bailey, H Young, PM Bloomfield, SR Meikle, D Glass, MJ Myers, TJ Spinks, CC Watson, P Luk, AM Peters, and T Jones. "ECAT ART – a continuously rotating PET camera: performance characteristics, initial clinical studies, and installation considerations in a nuclear medicine department", *Eur. J. Nucl. Med.* **24**, 6-15 (1997).
- TF Budinger. "PET Instrumentation: What are the limits? ", *Seminars in Nuclear Medicine*, Vol. XXVIII, no. 3, 247-267 (1998).
- JT Bushberg, JA Seibert, EM Leidholdt, Jr., and JM Boone. *The Essential Physics of Medical Imaging*, second edition, Lippincott Williams & Wilkins, 2002.
- FH Dahey. "Data Acquisition in PET Imaging", *J. Nucl. Med. Technol.* **30**, 39-49 (2002).
- DJ Parker, CJ Broadbent, P Fowles, MR. Hawkesworth, and P Mcneil. "Positron emission particle tracking—A technique for studying flow within engineering equipment," *Nucl. Instrum. Methods Phys. Res. A* **326**, 592-607 (1993).
- DJ Parker, RN Forster, P Fowles, and PS Takhar. "Positron emission particle tracking using the new Birmingham positron camera," *Nucl. Instrum. Methods Phys. Res. A* **477**, 540-545 (2002).
- G Tarantola, F Zito, and P Gerundini. "PET Instrumentation and Reconstruction Algorithms in Whole-Body Applications", *J. Nucl. Med.* **44**, 756-769 (2003).
- TG Turkington. "Introduction to PET Instrumentation", *J. Nucl. Med. Technol.* **29**, 1-8 (2001).
- PE Valk, DL Bailey, DW Townsend, and MN Maisey. *Positron Emission Tomography: Basic Science and Clinical Practice*, Springer-Verlag London Ltd, 69-90 (2003).
- T Xu, JT Wong, PM Shikhaliev, JL Ducote, MS Al-Ghazi, and S Molloy. "Real-time tumor tracking using implanted positron emission markers: Concept and simulation study", *Med. Phys.* **33**, 2598-2609 (2006).

